

CONTROL OF FWT EQUIPPED BY A PERMANENT MAGNET SYNCHRONOUS GENERATOR

Contents

3.1	Introduction	85
3.2	Model of FWT with the electric machine	86
3.2.1	Model of the permanent magnet synchronous generator	86
3.2.2	Model of the whole system	89
3.3	Control problem statement	91
3.3.1	Rotor speed reference	92
3.3.2	Quadratic current reference	92
3.3.3	Direct current reference	93
3.4	Control algorithms application	93
3.4.1	Baseline gain-scheduling PI controller	96
3.5	Simulations and analysis	96
3.6	Conclusion	104

3.1 Introduction

In Chapter 2, several adaptive high order sliding mode control algorithms have been applied on the FWT in Region III. Thanks to these novel approaches, both the power variation and the platform pitch motion are compared with the GSPI controller (J. Jonkman 2008b). These results have been obtained based on the fact that the generator torque is supposed to be fixed at its rated value, the power regulation being achieved by the rotor speed regulation. In fact, no model and control of electrical generator is considered.

In the current chapter, a permanent magnet synchronous generator (PMSG) is taken into consideration, and two adaptive versions of super-twisting controllers are applied to the FWT equipped

by a PMSG. The control is not only acting on the aero/hydrodynamic part, but also considers the electrical part that has not been made in previous chapter. Hence, both the collective blade pitch control and the generator torque control are now considered. In the sequel, the reference generator torque is no longer constant at the rated value, but is now varying with the rotor speed in order to guarantee a better regulation of power. The reference rotor speed is varying with platform pitch velocity as perennially to ensure attenuation of the platform pitch motion. Moreover, since a generator is considered, the limitation of oscillations of the electromagnetic torque is also taken in to consideration. In summary, the main contributions of this chapter are:

- modeling of the PMSG and interaction it with the FWT model;
- description of the control of the floating wind turbine equipped by a PMSG;
- application of the proposed adaptive HOSM controllers to the FAST software including PMSG model in SIMULINK, and performance analysis.

3.2 Model of FWT with the electric machine

3.2.1 Model of the permanent magnet synchronous generator

The PMSG is used by an industrial way, since it has features of high efficiency, high reliability, and low maintenance level (Haque, Negnevitsky, and Muttaqi 2010; Benelghali, Benbouzid, and Charpentier 2012; Keysan, McDonald, and Mueller 2011). Those features appear to be especially suitable for the wind turbines power generation systems, and the synchronous generator plays a crucial role in transforming mechanical energy into electrical energy. The mathematical model of the synchronous generator is a prerequisite in order to design the control algorithms. In this section, models of the PMSG in both the three-phase plane and the rotary $d-q$ reference frame, are recalled.

Three-phase model of PMSG (Guenoune 2018; Glumineau and De León-Morales 2015)

In order to establish a simplified model of the PMSG, consider the following assumptions

- the stator windings are balanced with a sinusoidal distribution of the magneto-motive force;
- the saturation of the magnetic circuit is neglected;
- Eddy currents, hysteresis phenomena and rotor saliency are neglected.

The machine voltages in the three-phase frame of reference (a, b, c) of the stator are given by

$$\begin{bmatrix} V_a \\ V_b \\ V_c \end{bmatrix} = R_s \begin{bmatrix} i_a \\ i_b \\ i_c \end{bmatrix} + \frac{d}{dt} \begin{bmatrix} \phi_a \\ \phi_b \\ \phi_c \end{bmatrix} \quad (3.1)$$

with

$$\begin{bmatrix} \phi_a \\ \phi_b \\ \phi_c \end{bmatrix} = L_s \begin{bmatrix} i_a \\ i_b \\ i_c \end{bmatrix} + \phi_f \begin{bmatrix} \cos(\theta) \\ \cos(\theta - \frac{2\pi}{3}) \\ \cos(\theta + \frac{2\pi}{3}) \end{bmatrix} \quad (3.2)$$

where

- $[V_a, V_b, V_c]^T$ the stator phase voltages;
- $[i_a, i_b, i_c]^T$ the stator phase currents;
- $[\phi_a, \phi_b, \phi_c]^T$ the stator fluxes;
- R_s the stator resistance. The resistances on the three-phase are assumed to be identical;
- ϕ_f the magnetic fluxes of the magnets;
- θ the angular position of the generator rotor;
- L_s the inductance matrix (3×3) composed by constant term and variable term such that

$$L_s = L_{s0} + L_{sv} \quad (3.3)$$

with

$$L_{s0} = \begin{bmatrix} L_{s0} & M_0 & M_0 \\ M_0 & L_{s0} & M_0 \\ M_0 & M_0 & L_{s0} \end{bmatrix} \quad (3.4)$$

and

$$L_{sv} = \begin{bmatrix} \cos(2\theta_e) & \cos(2\theta_e - \frac{2\pi}{3}) & \cos(2\theta_e + \frac{2\pi}{3}) \\ \cos(2\theta_e - \frac{2\pi}{3}) & \cos(2\theta_e + \frac{2\pi}{3}) & \cos(2\theta_e) \\ \cos(2\theta_e + \frac{2\pi}{3}) & \cos(2\theta_e) & \cos(2\theta_e - \frac{2\pi}{3}) \end{bmatrix} \quad (3.5)$$

where L_{s0} , L_{sv} and M_0 are the proper and mutual inductances respectively. These terms are constant. Finally, $\theta_e = p\theta$ with p the number of poles of the generator.

Two-phase ($d - q$ frame) model of PMSG (Glumineau and De León-Morales 2015; Soliman et al. 2018)

The expressions of PMSG model in the three-phase reference frame are not easy to manipulate and for the control design. The three-phase-two-phase transformation makes it possible to obtain a simplified representation of the PMSG in a plane equivalent to two axes. By using the so-called Park's transformations (Park 1929; Vas 1998), the a , b , c three-phase currents of the stator are transferred to the direct axis (d-axis), quadrature axis (q-axis) and the zero axis (0-axis) perpendicular to the $d - q$ plane along with the rotor rotation, thus simplifying the analysis of synchronous machine. The standard model of PMSG in the $d - q$ frame reads as

$$\begin{aligned} V_d &= R_s i_d L_d \frac{di_d}{dt} - p\Omega_g L_q i_q \\ V_q &= R_s i_q L_q \frac{di_q}{dt} + p\Omega_g L_d i_d + p\phi_f \Omega_g \end{aligned} \quad (3.6)$$

with

- i_d and i_q the currents along the $d - q$ axes respectively;
- V_d and V_q the voltages along the $d - q$ axes respectively;
- L_d and L_q the inductances along the $d - q$ axes respectively; in this work, one assumes $L_d = L_q$;
- ϕ_f the permanent-magnet flux linkage;
- Ω_g the generator speed.

The circuit of PMSG on $d - q$ frame can be shown schematically in Figure 3.1, with E_d and E_q the counter electric potentials of d and q axes respectively, and reading as

$$\begin{aligned} E_d &= 0 \\ E_q &= p\Omega_g \phi_f \end{aligned} \quad (3.7)$$

The generator electromagnetic torque is given by (Soliman et al. 2018)

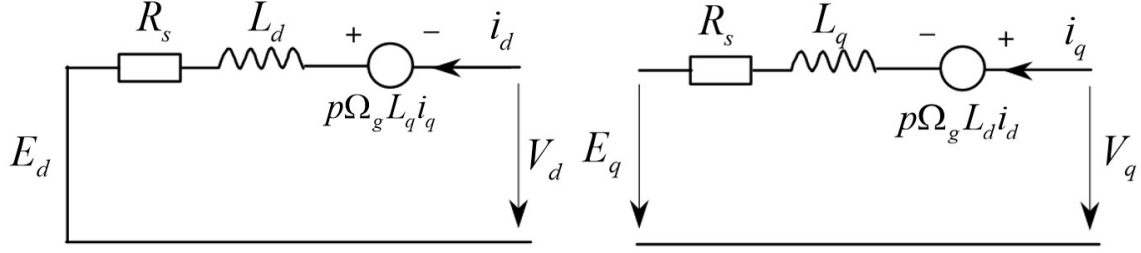


Figure 3.1 – Equivalent circuit of PMSG in the $d-q$ frame (Yin et al. 2007). **Left.** d -axis equivalent circuit. **Right.** q -axis equivalent circuit.

$$\Gamma_g = \frac{3}{2}p(\phi_f i_q + (L_q - L_d)i_d i_q) \quad (3.8)$$

Since the inductances along the $d-q$ axes are equal, the generator torque reads as

$$\Gamma_g = \frac{3}{2}p\phi_f i_q \quad (3.9)$$

Notice that Γ_g directly depends on q -axis current i_q and so could be controlled by i_q . This feature will be used in the sequel by a control point-of-view.

3.2.2 Model of the whole system

From (3.6), one gets the dynamics of $d-q$ currents

$$\begin{aligned} \frac{di_d}{dt} &= -\frac{R_s}{L_d}i_d + \frac{pL_q}{L_d}\Omega_g i_q + \frac{1}{L_d}V_d \\ \frac{di_q}{dt} &= -\frac{R_s}{L_q}i_q - \frac{pL_d}{L_q}\Omega_g i_d - \frac{p\phi_f}{L_q}\Omega_g + \frac{1}{L_q}V_q \end{aligned} \quad (3.10)$$

Then, the PMSG system can be written as

$$\dot{x}_{em} = f_{em}(x_{em}, \Omega_g) + g_{em}u_{em} \quad (3.11)$$

with $x_{em} = [i_d \ i_q]^T$ the state vector and $u_{em} = [V_d \ V_q]^T$ the input vector. The functions $f_{em}(x_{em}, \Omega_g)$ and g_{em} are defined respectively by

$$f_{em}(x_{em}, \Omega_g) = \begin{bmatrix} -\frac{R_s}{L_d}i_d + \frac{pL_q}{L_d}\Omega_g i_q \\ -\frac{R_s}{L_q}i_q - \frac{pL_d}{L_q}\Omega_g i_d - \frac{p\phi_f}{L_q}\Omega_g \end{bmatrix} \quad (3.12)$$

$$g_{em} = \begin{bmatrix} \frac{1}{L_d} & 0 \\ 0 & \frac{1}{L_q} \end{bmatrix} \quad (3.13)$$

Recalling the reduced FWT model (1.13) detailed in Section 1.3.1, as previously explained, in a large operating domain, the model of FWT can be defined as ¹

$$\dot{x}_{wt} = f_{wt}(x_{wt}, t) + g_{wt}(t)u_{wt} \quad (3.14)$$

with $x_{wt} = [\varphi \ \dot{\varphi} \ \Omega_r]^T$, φ being the platform pitch angle and Ω_r the rotor speed. u_{wt} is the collective blade pitch angle β_{col} . $f_{wt}(x_{wt}, t)$ is unknown but bounded function: it contains the properties of wind turbine in different operating point (the term $A_{Avg}(x, t)$ in (1.12)), the uncertainties of the system, the perturbations introduced by wind (the term $B_{dAvg}(x, t) \cdot \delta$ in (1.12)), waves and other external environments; $g_{wt}(t)$ is supposed to be unknown but bounded input function.

Notice that system (3.11) and (3.14) are linked by the the rotation speeds of generator/rotor with $\Omega_g = n_g \Omega_r$. Thus, combining the reduced model of FWT (3.14) and the model of PMSG (3.11), the whole system model can be viewed as the following nonlinear multiple-input multiple-output (MIMO) system

$$\dot{x} = \underbrace{\begin{bmatrix} f_{wt}(x_{wt}, t) \\ f_{em}(x_{em}) \end{bmatrix}}_{f(x, t)} + \underbrace{\begin{bmatrix} g_{wt}(t) & \mathbf{0}_{1 \times 2} \\ \mathbf{0}_{2 \times 1} & g_{em}(x_{em}) \end{bmatrix}}_{g(x, t)} \cdot \underbrace{\begin{bmatrix} \beta_{col} \\ V_d \\ V_q \end{bmatrix}}_u \quad (3.15)$$

with the state vector x and the input vector u of the whole system defined as

$$x = \begin{bmatrix} \varphi \\ \dot{\varphi} \\ \Omega_r \\ i_d \\ i_q \end{bmatrix}, \quad u = \begin{bmatrix} \beta_{col} \\ V_d \\ V_q \end{bmatrix} \quad (3.16)$$

Notice that $f(x, t)$ and $g(t)$ can be viewed as uncertain functions given that

- $f(x, t)$ depends on the perturbation term $B_{dAvg}(x, t) \cdot \delta$ and electrical parameters (resistances, inductance, ...) that can strongly vary especially versus temperature;

1. For a sake of clarity, notice the state vector and the input of the reduced FWT model as x_{wt} and u_{wt} respectively.

- $g(t)$ depends on inductance.

3.3 Control problem statement

In the considered operating region (Region III), the control objectives of floating wind turbine are the regulation of the power at its rated value P_0 to avoid overload operation and protect the electric machine; the second objective consists in attenuating the platform pitch motion so as to protect mechanical structure. In Chapter 2, the power regulation is achieved by regulating the rotor speed Ω_r with generator torque supposed at its rated value. The generator torque control was not taken into consideration, namely, the generator torque was supposed to be perfectly maintained at Γ_{g0} . In this chapter, given that the PMSG is now combined, the power control is completed by torque control and rotor speed control. Two kinds of strategies are possible

- **constant torque:** as detailed in Chapter 2, the generator torque Γ_g is fixed at its rated value Γ_{g0} , the power regulation being then turned into rotor speed regulation according to the relation between the power, the torque and the rotor speed

$$P = n_g \Gamma_{g0} \Omega_r. \quad (3.17)$$

- **constant power:** the control is directly acting on the power. In this case, the generator torque is no longer fixed at its rated value, but is changing with respect to the rotor speed, in order to maintain the constant power output, *i.e.*

$$P_0 = n_g \Gamma_g \Omega_r. \quad (3.18)$$

These two approaches will be used in the sequel. It has been demonstrated that, for the baseline GSPI control, the constant power strategy results in a smaller power variation (obvious given that the power is directly controlled) but induces additional platform pitch motion and structure loads whereas the constant torque strategy increases power variation but gives better performances on platform pitch motion and structure loads (Larsen and Hanson 2007; J. Jonkman 2008a; H. Namik and K. Stol 2014).

In this chapter, the adaptive high order sliding mode controllers are based on the constant power

approach, whereas two baseline GSPI controllers are applied both the constant torque and constant power approach, and are used as comparison objects.

3.3.1 Rotor speed reference

As explained in Chapter 2, in order to both regulate the rotor speed and reduce the platform pitch motion by CBP approach, a solution is to define the desired rotor speed Ω_r^* as a function of platform pitch velocity $\dot{\varphi}$

$$\Omega_r^* = \Omega_{r0} - k\dot{\varphi} \quad (3.19)$$

with $k > 0$.

3.3.2 Quadratic current reference

As mentioned previously, generator torque control is applied in this chapter. From (3.9), one finds that the generator torque can be modified by the quadratic current i_q , and then acting on the power output. Hence, according to the two control approaches (constant torque (3.17) and constant power (3.18)), the desired quadratic current i_q^* for the two strategies is designed as follows.

- **constant torque:** suppose that the generator torque is fixed at its rated value Γ_{g0} . According to (3.9), one has

$$\Gamma_{g0} = \frac{3}{2}p\phi_f i_q \quad (3.20)$$

Then, the reference quadratic current i_q^* is defined as

$$i_q^* = \frac{2\Gamma_{g0}}{3p\phi_f} \quad (3.21)$$

in order to keep a constant generator torque²;

- **constant power:** in order to maintain a constant (rated) power output, the following equation based on (3.9) and (3.18) is established

$$\frac{P_0}{n_g\Omega_r} = \frac{3}{2}p\phi_f i_q \quad (3.22)$$

Therefore, if the current i_q tracks the following reference

$$i_q^* = \frac{2P_0}{3n_g\Omega_r p\phi_f}, \quad (3.23)$$

2. In this case, if Ω_r is forced to Ω_r^* with reduced platform pitch motion, $\Omega_r = \Omega_{r0}$. Then, the power equals to its rated value $P_0 = n_g\Gamma_{g0}\Omega_{r0}$.

the power output is limited to its rated value.

3.3.3 Direct current reference

The oscillations of the electromagnetic torque can amplify the fatigue loads on the mechanical shaft, thus affecting the quality of the energy produced. In order to limit this drawback, a solution consists in forcing the direct current i_d to zero (Glumineau and De León-Morales 2015; Z. Chen 2013). The reference of this current is given by

$$i_d^* = 0. \quad (3.24)$$

3.4 Control algorithms application

From the control objectives detailed in the previous section, the control input vector u and the output vector y of the whole system read as (i_q^* used here being defined by (3.23))

$$u = \begin{bmatrix} \beta_{col} \\ V_d \\ V_q \end{bmatrix}, \quad y = \begin{bmatrix} y_1 \\ y_2 \\ y_3 \end{bmatrix} = \begin{bmatrix} \Omega_r - \Omega_r^* \\ i_d - i_d^* \\ i_q - i_q^* \end{bmatrix} \quad (3.25)$$

Recall that the control objective of is to force y to 0 (in practice, this objective is to force y to a vicinity of 0). From (3.15), the relative degree vector of the three outputs y_1 , y_2 and y_3 with respect respectively to β_{col} , V_d and V_q is equal to $[1, 1, 1]$. As a consequence, the sliding vector S is defined as

$$S = \begin{bmatrix} S_1 \\ S_2 \\ S_3 \end{bmatrix} = \begin{bmatrix} y_1 \\ y_2 \\ y_3 \end{bmatrix} = \begin{bmatrix} \Omega_r - \Omega_{r0} + k\dot{\varphi} \\ i_d \\ i_q - \frac{2P_0}{3n_g\Omega_r p\phi_f} \end{bmatrix} \quad (3.26)$$

Dynamics of S_1 . According to (3.19), (3.25) and (3.26), S_1 -dynamics reads as

$$\dot{S}_1 = \dot{\Omega}_r + k\ddot{\varphi} \quad (3.27)$$

Recalling (1.4), (1.6) and (3.9), one gets

$$\dot{S}_1 = \frac{1}{2J} \underbrace{\left(\frac{C_p(\lambda, \beta_{col})}{\lambda} \rho\pi R^2 V^3 - 3n_g p\phi_f i_q \right)}_{\dot{\Omega}_r} + k\ddot{\varphi} \quad (3.28)$$

Notice that $\dot{\Omega}_r$ depends on the power coefficient C_p that is not well-known³. However, according to (1.3), it can be numerically shown that the power coefficient C_p can be approximated as

$$C_p = C_{p1}(\cdot) + C_{p2}(\cdot)\beta_{col} \quad (3.29)$$

Then, the dynamic of Ω_r can be rewritten as

$$\dot{\Omega}_r = a_{\Omega_r}(\cdot) + b_{\Omega_r}(\cdot)\beta_{col} \quad (3.30)$$

with a_{Ω_r} and b_{Ω_r} unknown but bounded functions. On the other hand, recalling the reduced linear model detailed in Subsection 1.3.1, $\dot{\varphi}$ is a not well-known dynamics. For a large operating domain, one has⁴

$$\dot{\varphi} = a_{\varphi}(\cdot) + b_{\varphi}(\cdot)\beta_{col} \quad (3.31)$$

with a_{φ} and b_{φ} unknown but bounded functions. As a consequence, the dynamic of S_1 can be rewritten as

$$\dot{S}_1 = a_1(\cdot) + b_1(\cdot)\beta_{col} \quad (3.32)$$

with $a_1 = a_{\Omega_r} + a_{\varphi}$, $b_1 = b_{\Omega_r} + b_{\varphi}$ unknown but bounded functions.

Dynamics of S_2 . According to (3.10), (3.24), (3.25) and (3.26), S_2 -dynamics reads as

$$\dot{S}_2 = -\frac{R_s}{L_d}i_d + \frac{pL_q}{L_d}\Omega_g i_q + \frac{1}{L_d}V_d \quad (3.33)$$

It can be rewritten as

$$\dot{S}_2 = a_2(\cdot) + b_2(\cdot)V_d \quad (3.34)$$

Notice that, in (3.10), one supposes that each parameter is composed by a known nominal part and unknown uncertainty one (for example, the resistance R_s can be written as $R_s = R_{sn} + \Delta R_s$, R_{sn} being the nominal value and ΔR_s the associated uncertainty). Then, one gets $a_2 = a_{2n} + \Delta a_2$ and $b_2 = b_{2n} + \Delta b_2$ with a_{2n} and b_{2n} the nominal part reading as

$$\begin{aligned} a_{2n} &= -\frac{R_s}{L_d}i_d + \frac{pL_q}{L_d}\Omega_g i_q \\ b_{2n} &= \frac{1}{L_d} \end{aligned} \quad (3.35)$$

3. C_p depends on the fitting coefficients $c_1 - c_5$. These coefficients are not well-known and introduce uncertainties (see Subsection 1.2.2).

4. Indeed, it is clear that $\dot{\Omega}_r$ can be obtained by this way. However, in this work, $\dot{\Omega}_r$ is obtained based on the physical model in order to claim that the physical model and the linearized model could get the same result.

Dynamics of S_3 . According to (3.10), (3.23), (3.25) and (3.26), S_3 -dynamics reads as

$$\dot{S}_3 = -\frac{R_s}{L_q}i_q - \frac{pL_d}{L_q}\Omega_g i_d - \frac{p\phi_f}{L_q}\Omega_g - \frac{2P_0\dot{\Omega}_r}{3n_g p\phi_f \Omega_r^2} + \frac{1}{L_q}V_q \quad (3.36)$$

It depends on the dynamics of Ω_r that is not well-known and coupled with the blade pitch angle β_{col} . However, numerical analysis in the operating domain shows that the influence of β_{col} is very limited on S_3 -dynamics. Therefore, considering the term in \dot{S}_3 that contains $\dot{\Omega}_r$, as a bounded perturbation, it gives

$$\dot{S}_3 = a_3(\cdot) + b_3(\cdot)V_q \quad (3.37)$$

with $a_3 = a_{3n} + \Delta a_3$ and $b_3 = b_{3n} + \Delta b_3$. The terms a_{3n} and b_{3n} read as

$$\begin{aligned} a_3 &= -\frac{R_s}{L_q}i_q - \frac{pL_d}{L_q}n_g\Omega_g i_d - \frac{p\Phi_f}{L_q}n_g\Omega_g \\ b_{3n} &= \frac{1}{L_q} \end{aligned} \quad (3.38)$$

Therefore, the control input reads as

$$u = \begin{bmatrix} \beta_{col} \\ V_d \\ V_q \end{bmatrix} = \begin{bmatrix} v_1 \\ \frac{1}{b_{2n}}(-a_{2n} + v_2) \\ \frac{1}{b_{3n}}(-a_{3n} + v_3) \end{bmatrix} \quad (3.39)$$

with v_1 , v_2 and v_3 defined as adaptive super-twisting algorithms (2.11)

$$\begin{bmatrix} v_1 \\ v_2 \\ v_3 \end{bmatrix} = \begin{bmatrix} -k_{11}|S_1|^{\frac{1}{2}}\text{sign}(S_1) - \int_0^t k_{12}\text{sign}(S_1)d\tau \\ -k_{21}|S_2|^{\frac{1}{2}}\text{sign}(S_2) - \int_0^t k_{22}\text{sign}(S_2)d\tau \\ -k_{31}|S_3|^{\frac{1}{2}}\text{sign}(S_3) - \int_0^t k_{32}\text{sign}(S_3)d\tau \end{bmatrix} \quad (3.40)$$

with the gains k_{11}, k_{21}, k_{31} and k_{12}, k_{22}, k_{32} defined from (2.21) for ASTW, and from (2.27) for SAST⁵.

5. For the controller gains of SAST in this chapter, $k_{i1} = 2L$, $k_{i2} = L^2/2$, $i \in \{1, 2, 3\}$.

3.4.1 Baseline gain-scheduling PI controller

The baseline controller used in this paper for the rotor speed control loop is the famous GSPI controller (J. Jonkman 2008b; J. Jonkman, Butterfield, et al. 2009). Then, the control input

$$v_1 = n_g K_p (\Omega_r - \Omega_{r0}) + n_g K_i \int_0^t (\Omega_r - \Omega_{r0}) d\tau \quad (3.41)$$

with K_p and K_i obtained for different operating points and scheduled as functions of blade pitch angle (see Subsection 2.5.3). Furthermore, the gains are detuned in order to avoid platform pitch negative damping; details can be found in (J. Jonkman 2008b). Recall that the tuning of such controller is a huge and fastidious task given the large operating domain. For the generator torque/power control loop, two kinds of strategies (H. Namik and K. Stol 2014) are used in the sequel

- **Constant power control.** The control V_d and V_q are defined by (3.39) with

$$\begin{aligned} v_2 &= K_{p2} S_2 + K_{i2} \int_0^t S_2(\tau) d\tau \\ v_3 &= K_{p3} S_3 + K_{i3} \int_0^t S_3(\tau) d\tau \end{aligned} \quad (3.42)$$

with S_2 and S_3 defined by (3.26).

- **Constant torque control.** As detailed previously, the generator torque is forced to its rated Γ_{g0} , *i.e.* $\Gamma_g^* = \Gamma_{g0}$. One gets

$$i_q^* = \frac{2\Gamma_{g0}}{3p\phi_f}$$

Hence, similar PI controllers as (3.42) are used with S_2 defined as (3.26) and S_3 as

$$S_3 = i_q - \frac{2\Gamma_{g0}}{3p\phi_f} \quad (3.43)$$

3.5 Simulations and analysis

The simulations have been carried out assuming that the FAST 5MW OC3-Hywind floating wind turbine model is equipped with a permanent magnet synchronous generator. The parameters of the PMSG are displayed in Table 3.1 and the characteristics of the FWT have been detailed in Chapter 1. All simulations are made by co-simulation between all DOFs enabled FAST model and SIMULINK, the simulation time being 600 seconds. Euler integration algorithm is used with a fixed step of 0.0125 second. Four control strategies based on the control input defined by (3.39) are presented and compared in the sequel

- **GSPI1+PI:** rotor speed control GSPI (3.41) with *constant torque* strategy power/direct current PI control (3.42), S_2 and S_3 being defined by (3.26);

- **GSPI2+PI:** rotor speed control GSPI (3.41) with *constant power* strategy power/direct current control (3.42), S_2 being defined by (3.26) and S_3 by (3.43);
- **ASTW:** super-twisting algorithm (3.40) with gain adaptation law defined by (2.21);
- **SAST:** super-twisting algorithm (3.40) with gain adaptation law defined by (2.27).

Table 3.1 – PMSG parameters

Parameters	Value
Rated power P_0	5 MW
Rated generator speed	1173.7 rpm
Stator resistance R_s	1.06 Ω
Stator inductance L_d, L_q	14.29 mH
Flux linkage ϕ_f	8.6 Wb
No. of pole pairs p	5
Maximum generator torque	47,402.91 N·m
Maximum generator torque rate	15000 N·m/s

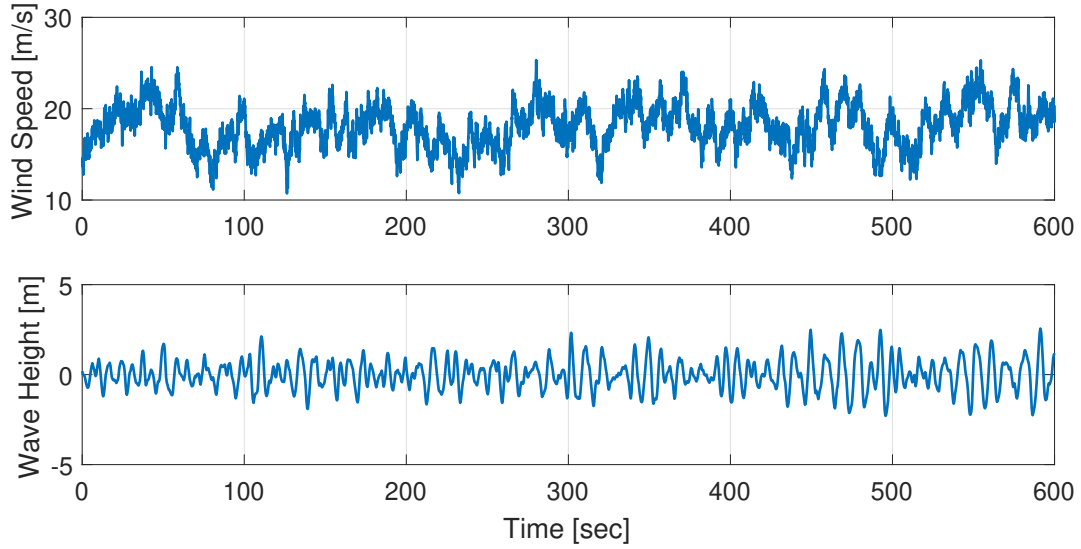
All the simulations are made under the same conditions (see Figure 3.2)

- 18m/s stochastic wind with 15% turbulence intensity;
- irregular wave with significant height of 3.25m, peak spectral period of 9.7s.

Recall that, a saturation on blade pitch angle and an associated rate limiter are introduced in order to ensure more accurate simulations versus real system. Furthermore, perturbations were added on i_d and i_q by a band-limited white noise block of SIMULINK with noise power equal to 20 and 30 respectively, both of them having a sampling time equal to 5 ms. Finally, as explained just after (3.34), parametric uncertainties are considered (Table 3.2) which introduce bias in the control law through the functions a_{2n} , b_{2n} , a_{3n} and b_{3n} (see (3.35)-(3.38)), so as to check the robustness of the closed-loop system. The controller gains of the two GSPI controllers are the same and composed

Table 3.2 – Parametric uncertainties of PMSG

Uncertain parameters	Uncertainty amplitudes (%)
Stator resistance R_s	-25
Stator inductance L_d	20
Flux linkage ϕ_f	-20


 Figure 3.2 – Wind speed (**top**) and wave height (**bottom**) versus time (*sec.*).

by two parts: the controller gains for the rotor speed control loop K_p and K_i are the same as in (J. Jonkman 2008b). The gains for the electrical part are displayed in Table 3.3 whereas the controller gains of ASTW and SAST are shown in Table 3.4 and the parameter k of sliding variable S_1 in (3.26) is equal to 16.7. All these gains have been tuned in order to get the best performances.

Table 3.3 – Controller gains of PI

Controlled variables	Proportional gain	Integral gain
Direct current i_d	500	10^4
Quadratic currents i_q	200	10^4

Table 3.4 – Controller gains of ASTW and SAST

Gains	Parameters of ASTW	Parameters of SAST
k_{11}, k_{12}	$\alpha_m = 10^{-5}, \omega = 0.001, \chi = 2, \epsilon = 0.03, \mu = 0.05, \eta = 10^{-5}$	$l_m = 10^{-5}, \mu = 0.06$
k_{21}, k_{22}	$\alpha_m = 1, \omega = 200, \chi = 2, \epsilon = 200, \mu = 0.05, \eta = 10$	$l_m = 0.01, \mu = 0.05$
k_{31}, k_{32}	$\alpha_m = 100, \omega = 40, \chi = 2, \epsilon = 300, \mu = 0.1, \eta = 10$	$l_m = 0.01, \mu = 0.1$

Figure 3.3 shows the evolution of the main variables of the system; it gives a general view of the different controllers performances. These plots show that the four controllers are more or less efficient. In order to accurately analyzing the closed-loop system performances, recall the following performance indicators detailed in Chapter 1.

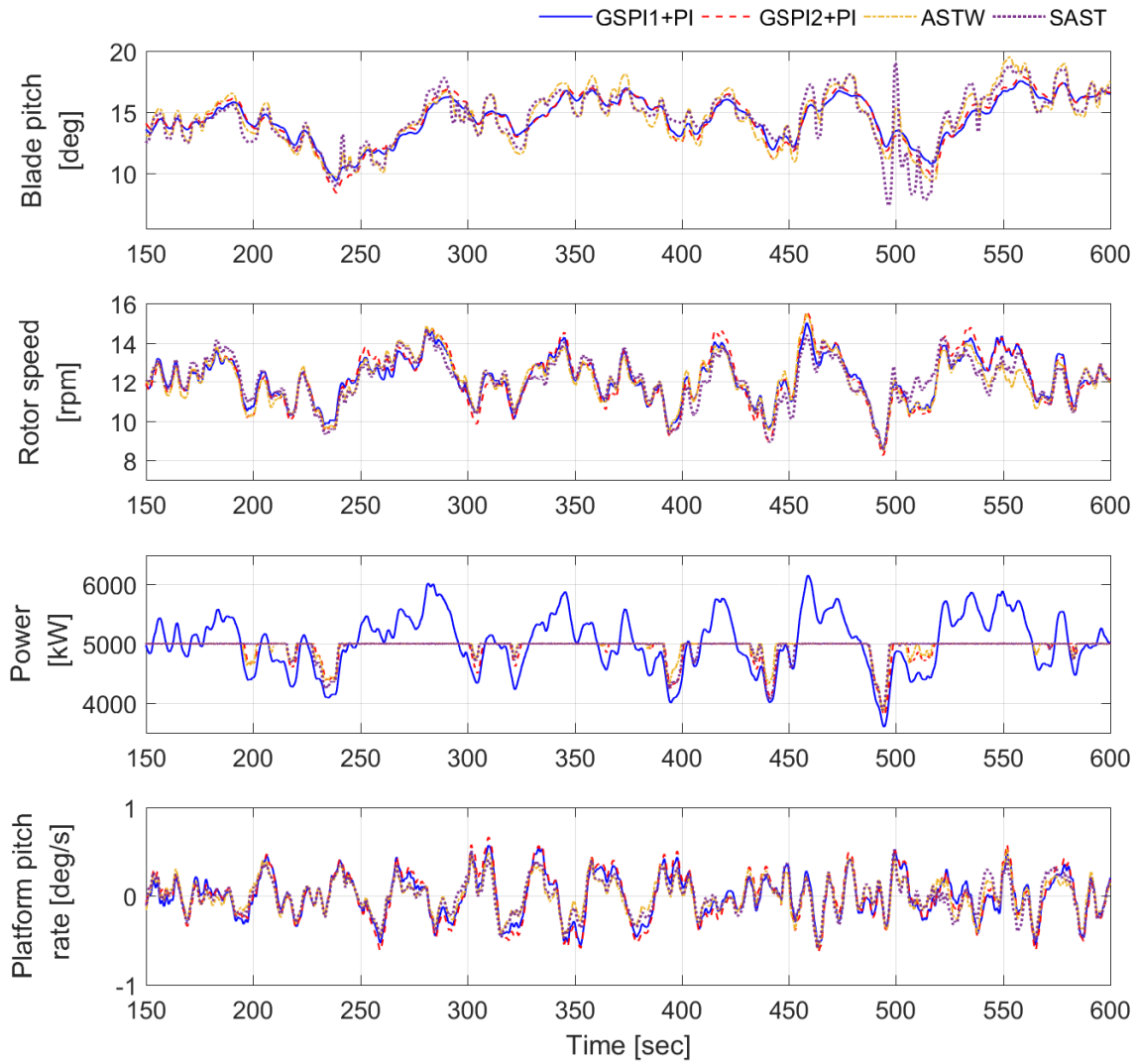


Figure 3.3 – Main variables of the FWT versus time (sec), obtained by GSPI1+PI (blue), GSPI2+PI (red), ASTW (yellow) and SAST (purple) controllers.

- root mean square (RMS) of the error between the actual and rated power, the RMS of platform roll, pitch, yaw and the RMS of platform pitch rate. For all these RMS values, the objective is to obtain the smallest values;
- variation (VAR) of the blade pitch angle; it indicates the level of blade pitch actuation: a high value implies its frequent use and is a key-indicator in order to detect chattering;
- damage equivalent load (DEL) of tower base (TB) moments in fore-aft, side-to-side and torsional directions, the DEL of blade root (BR) edge-wise and flap-wise moments, the DEL of fair-lead force (FF) and anchor force (AF) of 3 mooring lines. Such indicators evaluate the fatigue load of the structure, the objective being to obtain the smallest values.

All of these performance indicators are normalized with respect to GSPI1+PI controller such that, the normalized values for GSPI1+PI controller are equal to 1 as shown in Figures 3.4 and 3.5.

First-of-all, Figures 3.4 and 3.5 display that GSPI1+PI control (constant torque) reduces, versus GSPI2+PI solution, the platform pitch motion and turbine loads (such as tower base and blade flap-wise loads) but increases the power regulation error versus GSPI2+PI control (constant power). Notice that this latter point could damage the generator because the power can be over the rated one (see Figure 3.3). Such conclusions are in accordance with (H. Namik and K. Stol 2014). Furthermore, it is natural that the power tracking is better with constant power based control, than with constant torque based control. Concerning DEL of the three mooring lines, the results obtained by both the GSPI controllers are similar.

Concerning the nonlinear controllers, both of them reduce the power error (see Figure 3.4; -64% for ASTW, -60% for SAST) versus GSPI1+PI, without increasing platform pitch motion (see Figure 3.4: lower pitch rate, lower roll). Versus GSPI2+PI, ASTW and SAST allow getting a reduction of roll and pitch rate that is a key-point. From these two first remarks, one can conclude that both nonlinear controllers have the advantages of both GSPI controllers without their lacks.

Concerning DEL, the ASTW and SAST do not improve the tower base moments DEL (Figure 3.5-top) versus GSPI controllers, but they clearly improve the mooring lines DEL (Figure 3.5-bottom). That is also a key-point for the stability and the viability of the system.

To summarize, the ASTW and SAST are more efficient versus GSPI1+PI and GSPI2+PI, on the basis of power regulation and platform pitch motion reduction; improvement is also obtained for the mooring lines. However, the cost of such improvements is a more important use of the blade

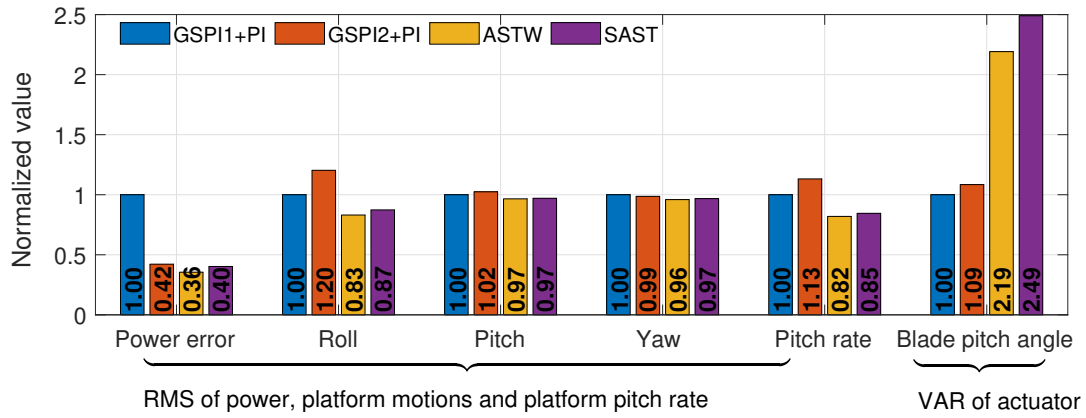


Figure 3.4 – Normalized RMS/VAR values of several performances indicators with GSPI1+PI (blue), GSPI2+PI (red), ASTW (yellow) and SAST (purple) controllers.

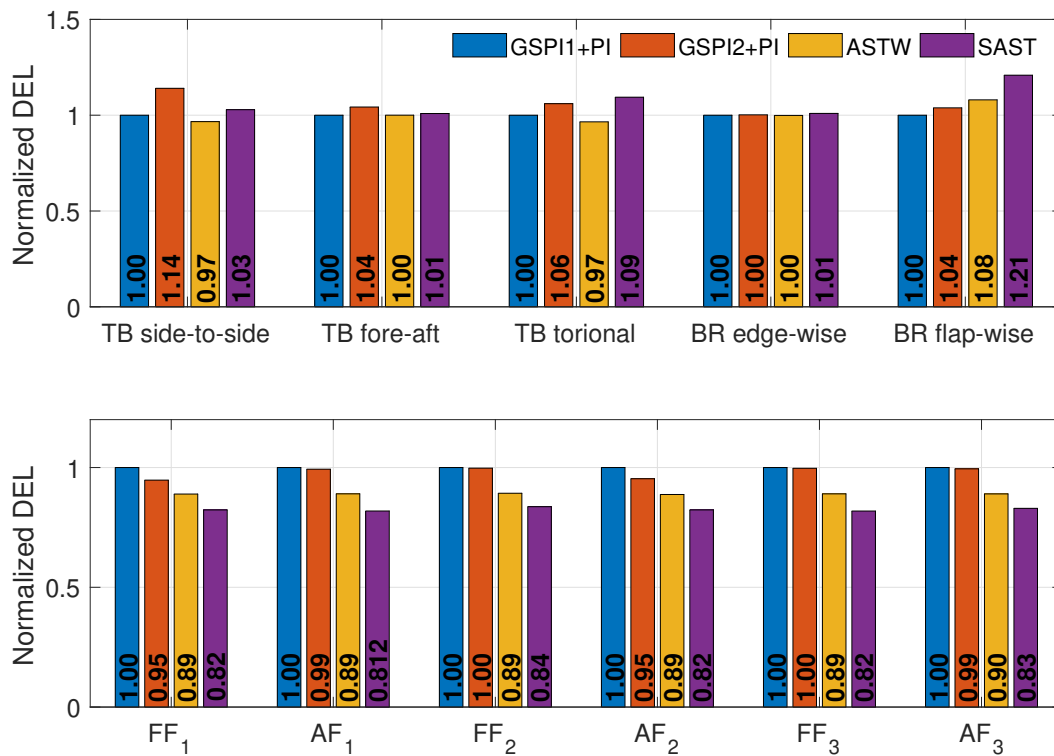


Figure 3.5 – Normalized DEL values of structure loads of GSPI1+PI (blue), GSPI2+PI (red), ASTW (yellow) and SAST (purple) controllers.

pitch actuator, *i.e.* the variations of ASTW and SAST versus GSPI are +119% and +149% respectively (see Figure 3.4). Nonetheless, since the blade pitch saturation and rate limiter are taken into consideration in the simulations, the controllers can be applied in practice.

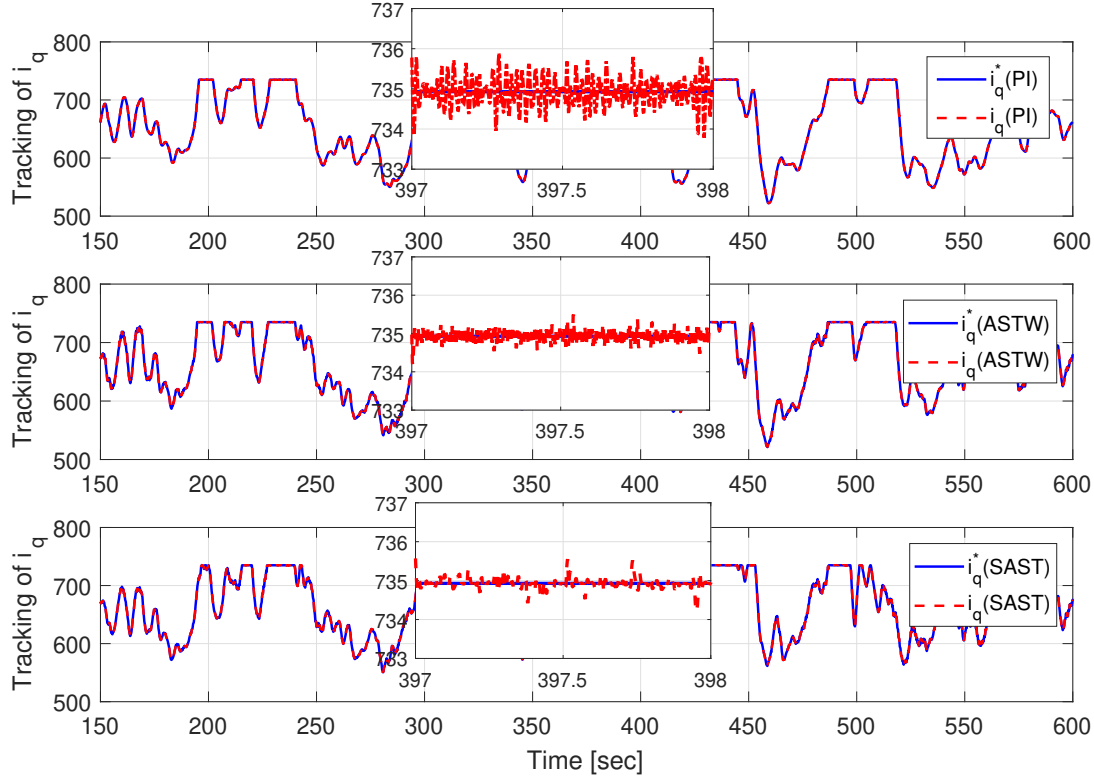


Figure 3.6 – Quadratic current i_q (A) and its reference versus time (sec.), obtained by PI (**top**), ASTW (**middle**) and SAST (**bottom**) controllers.

Concerning the electrical part, Figures 3.6- 3.7 show the tracking of i_q and i_d respectively. Since the generator torque is adjusted by the quadratic current i_q (see (3.9)), the tracking of i_q can be used to evaluate the performance of the torque control. Figures 3.7 and Table 3.5 display information on the tracking errors on both i_d and i_q . It appears that ASTW and SAST controllers allow to keep smaller the tracking error than both PI controllers. So, current (and torque) control is more efficient with super-twisting approach.

As shown by Figure 3.8, the gains of the ASTW and SAST controllers are dynamically adapted in order to keep accurate performances. It appears that all the gains, after a transient, converge towards a "steady state": they are evolving around an average value that is linked to the perturbations and uncertainties. Figure 3.9 shows the stator voltages and currents along the three phases frame

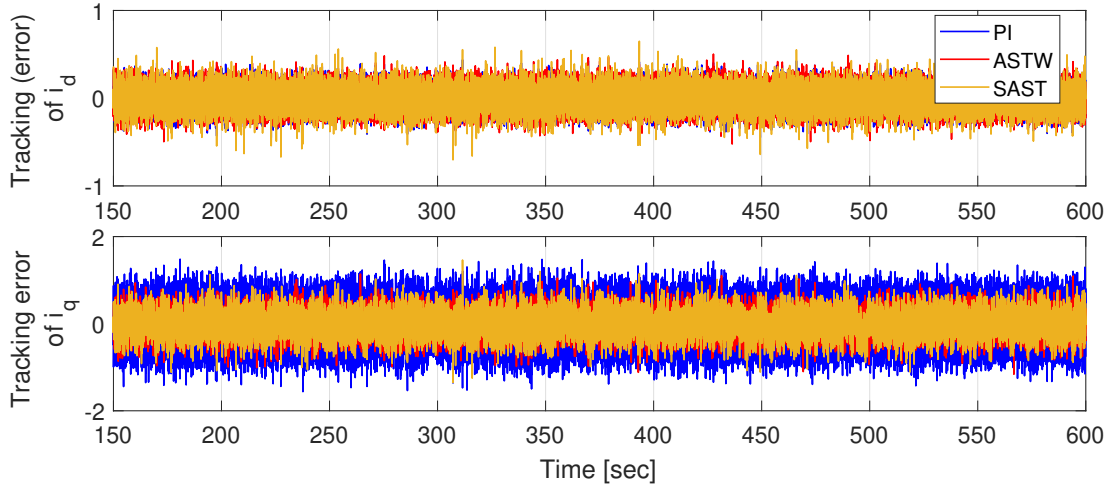


Figure 3.7 – Tracking error of currents i_d (A) and i_q (A) obtained by PI (blue), ASTW (red) and SAST (yellow) controllers versus time (sec.).

Table 3.5 – Mean tracking error of PMSG currents.

Controller	RMS of tracking error of i_d	RMS of tracking error of i_q
GSPI+PI1	0.0978	0.3596
GSPI+PI2	0.0978	0.3595
ASTW	0.0771	0.1535
SAST	0.0764	0.1512

obtained by both the super-twisting controllers. These signals appear to be realistic. Notice that the use of sliding mode controllers induce no high frequency oscillations (chattering) on these electrical variables.

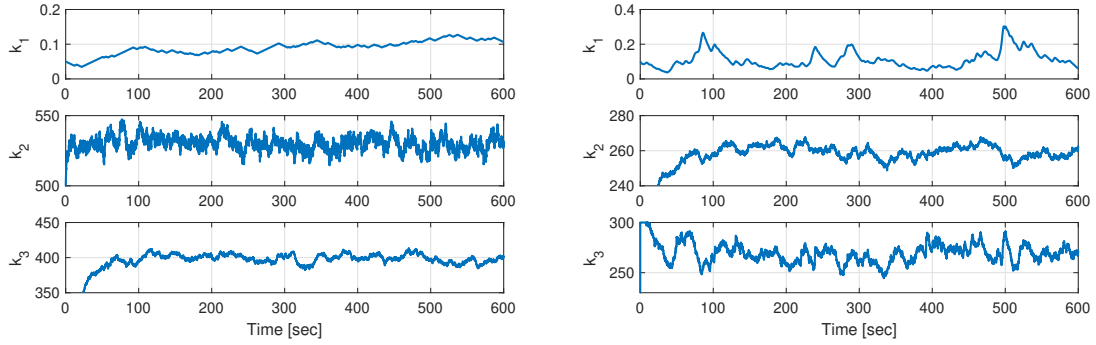


Figure 3.8 – Adaptive gains k_1 , k_2 and k_3 of ASTW (**left**) and SAST (**right**) versus time (sec).

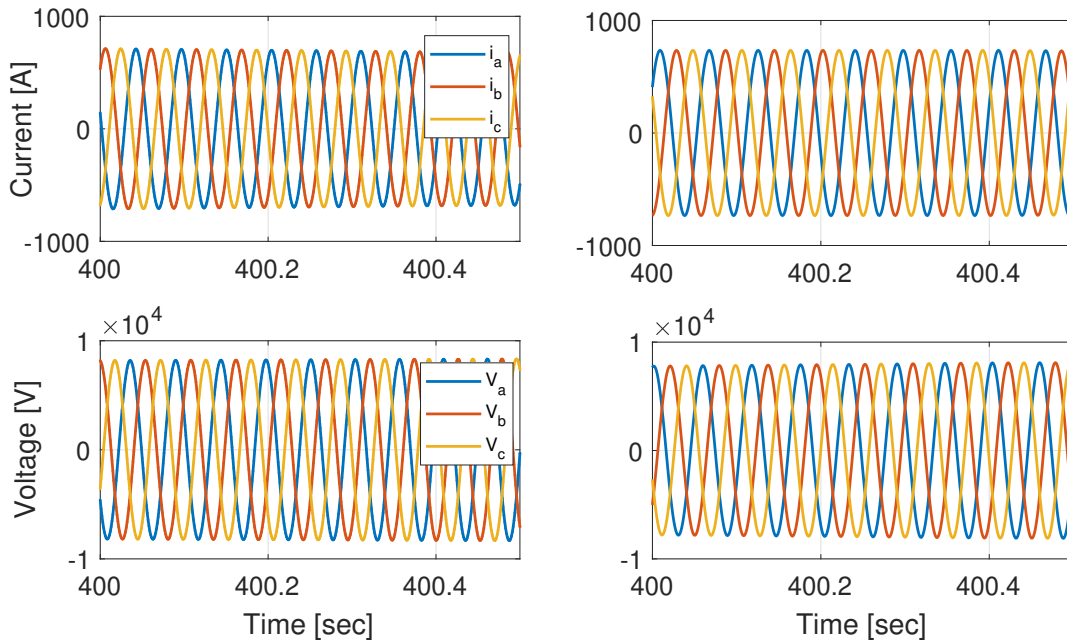


Figure 3.9 – Stator voltages (**top**) and currents (**bottom**) along the three phase frame versus time (sec.), by using ASTW (**left**) and SAST (**right**) controllers.

3.6 Conclusion

In this chapter, super-twisting based controllers with two kinds of gain adaptation algorithms have been for the first time applied to a floating wind turbine in above rated region, equipped by a per-

manent magnet synchronous machine. The control objectives are the regulation of the power output at its rated value and the reduction of the platform pitch motion, meanwhile, reducing the ripple effect of the generator. The two controllers are evaluated on a complete model including hydrodynamics, aerodynamics and electrical dynamics and allow to get better performances comparing with baseline controllers. Furthermore, the controller gains tuning effort is greatly reduced (especially with SAST) because these gains are dynamically adapted with uncertainties and perturbations.